



Article

Fabrication and Luminescent Properties of Er-Doped $\text{Sr}_5(\text{PO}_4)_3\text{F}$ Ceramics

Dmitry Permin ^{1,2,*} , Marsel Nazmutdinov ¹, Sergey Kurashkin ^{1,2}, Stanislav Balabanov ^{1,2} , Alexander Belyaev ^{1,2}, Anastasia Novikova ² and Vitaliy Koshkin ^{1,2}

¹ Faculty of Chemistry, N.I. Lobachevsky National Research University, 23 Gagarin Ave., 603022 Nizhny Novgorod, Russia

² G.G. Devyatykh Institute of Chemistry of High-Purity Substances, Russian Academy of Sciences, 49 Tropinin Str., 603137 Nizhny Novgorod, Russia

* Correspondence: permin@ihps-nnov.ru

Abstract: Nanopowders of strontium fluoroapatite $\text{Sr}_5(\text{PO}_4)_3\text{F}$ (SFAP) were synthesized using a co-precipitation method with different starting strontium compounds. Based on the data of XRD, BET and SEM measurements, the nitrate-derived powders were chosen as the least agglomerated. The SFAP powders were hot pressed at 1000 °C to ceramic samples with a transmittance up to 82% in a mid-IR region. The designed approach was adopted to prepare 2 mol % of Er-doped SFAP powders and ceramics. It was established that Er:SFAP ceramics have luminescence in the range of 1.5–1.7 μm, the intensity of which increases with the calcination temperature of the initial powders.

Keywords: SFAP; transparent ceramics; hot pressing; erbium



Citation: Permin, D.; Nazmutdinov, M.; Kurashkin, S.; Balabanov, S.; Belyaev, A.; Novikova, A.; Koshkin, V. Fabrication and Luminescent Properties of Er-Doped $\text{Sr}_5(\text{PO}_4)_3\text{F}$ Ceramics. *Inorganics* **2023**, *11*, 57. <https://doi.org/10.3390/inorganics11020057>

Academic Editor: Sergey Kuznetsov

Received: 19 November 2022

Revised: 22 January 2023

Accepted: 23 January 2023

Published: 25 January 2023



Copyright: © 2023 by the authors. Licensee MDPI, Basel, Switzerland. This article is an open access article distributed under the terms and conditions of the Creative Commons Attribution (CC BY) license (<https://creativecommons.org/licenses/by/4.0/>).

1. Introduction

Single crystals with an apatite structure doped with rare earth ions are known as laser materials with characteristics at the level of the best laser crystals and glasses [1]. The possibility of lasing in these media was found in the early 1970s [2]. However, the structural and luminescent properties of the most commonly used crystals of strontium fluorapatite $\text{Sr}_5(\text{PO}_4)_3\text{F}$ (SFAP) doped with ytterbium ions were studied towards the end of the 1990s and beginning of the 2000s, at which point, more features of laser diode excitation sources were realized [3–6]. In [4], Schaffers stated that the large emission and absorption cross sections of Yb^{3+} ions in the SFAP matrix (6.0×10^{20} and $10 \times 10^{20} \text{ cm}^2$, respectively) make diode pumping more cost-feasible for large laser systems, due to the reduced requirement on the diode brightness. Moreover, a long luminescence lifetime (1.14 msec), high damage threshold ($\geq 50 \text{ J/cm}^2$) and low losses ($< 10^{-3} \text{ cm}^{-1}$) make Yb:SFAP an attractive material for the creation of novel active media for lasers with a high repetition rate.

Since SFAP (also known as stronadelphite) has a non-cubic anisotropic crystal structure, its application as a laser material in the form of polycrystals (e.g., ceramics) is limited due to birefringence-induced losses of the transmitted light. At the same time, the higher mechanical properties of ceramics compared to single crystals, the possibility of increasing the concentration of the active additive and creating gradient-doped materials can lead to significant progress in the laser properties of solid-state laser materials, as has been shown for other laser ceramics, such as yttrium aluminum garnet [7], zinc selenide [8], calcium and strontium fluorides [9].

In this regard, attempts are being made to fabricate non-cubic optical ceramics with the fluorapatite structure. Akiyama et al. sintered laser-grade ytterbium doped calcium fluorapatite ceramics (Yb:FAP) with control of microdomain orientation [10,11]. In these studies, slip casting in a 1.4 T magnetic field and subsequent heat treatments in a hot isostatic press at 1600 °C were used. The orientation of the ceramic grains in one direction significantly reduced scattering losses.

Another approach to overcome scattering is to limit the grain size growth at the stage of ceramic sintering to a level of no more than ~ 100 nm. When the operating wavelengths are much higher than the grain sizes, the anisotropy of the material has no significant effect on the radiation propagation. However, achieving 100% ceramic density while maintaining such a small grain size is a challenging task. The diffusion processes responsible for pore healing and grain boundary migration occur simultaneously. Precise control of the characteristics of the powder and its subsequent consolidation method is necessary to achieve the desired ceramic structure. The main approach to the synthesis of FAP nanopowders is co-precipitation from solutions [12–15]. Consolidation methods with the application of external pressure, such as hot pressing [16–18] or spark plasma sintering (SPS) [14,19,20], are used to give additional sintering force while lowering the temperature and/or densification time to reduce the grain growth rate. Thus, Furuse et al. [19,20] obtained ceramic samples of fluorapatite and strontium–fluorapatite doped with ytterbium and neodymium ions (Yb:FAP and Nd:SFAP), and achieved laser generation with a slope efficiency of 4.6% and 6.5%, respectively. The same authors argued that Er:FAP ceramics can provide better performance for industrial and medical applications in the near-infrared because the scattering coefficient decreases with an increasing wavelength of generation.

To date, a series of Er³⁺-doped ceramic laser media, such as YAG [21], rare earth sesquioxides [22], calcium and strontium fluorides [23–25], has been produced for the 1–3 μm spectral region. Such materials have attracted a great deal of attention because of their potential as a component of eye-safe devices, optical fiber telecommunication, security system, LIDAR, etc. However, we have not found any information on the preparation of FAP or SFAP ceramics doped with erbium ions.

The aim of this study is to establish the conditions for sintering of transparent strontium fluorapatite ceramics and to evaluate the possibility of creating luminescent materials based on SFAP doped with erbium ions.

2. Results and Discussion

2.1. Effect of Strontium Source on the Morphology of SFAP Powders

It is known that the choice of the starting compound can have a significant effect on the morphology and structure of the precipitation product. To assess this effect, we chose strontium chloride, acetate and nitrate.

According to the XRD patterns shown in Figure 1, the synthesis product, regardless of the type of starting material, is a strontium fluorapatite phase; no reflections of impurity phases are observed.

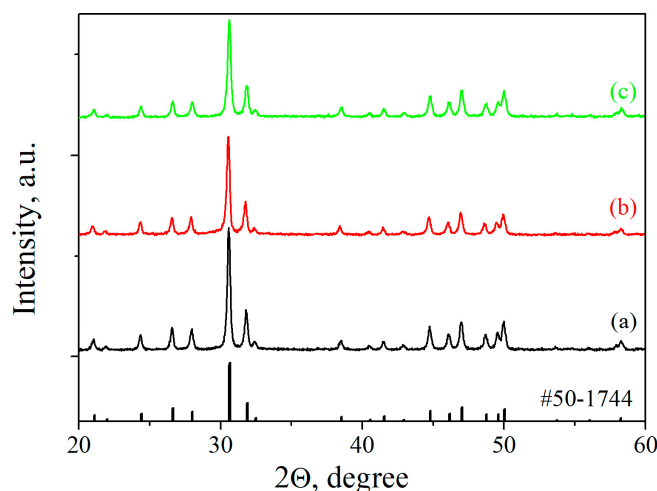


Figure 1. X-ray diffraction patterns of SFAP powders obtained with (a) acetate, (b) chloride, and (c) nitrate precursors. Vertical dashes—theoretical reflections for SFAP (PDF# 50-1744).

Figure 2 shows SEM micrographs of the obtained powders. In all cases, the powders consist of primary rounded particles with a size of 50–100 nm. SFAP powders synthesized from strontium acetate and nitrate appear to be less agglomerated compared to those obtained from strontium chloride. Presumably, complex anions (acetate, nitrate) shield particles more strongly when they are adsorbed on the surface of precipitated particles. Moreover, acetate and nitrate fragments during oxidative annealing in air give several gas molecules ($\text{CO}_2\text{-H}_2\text{O}$, $\text{NO}_2\text{-H}_2\text{O}$); therefore, the powder agglomeration becomes looser.

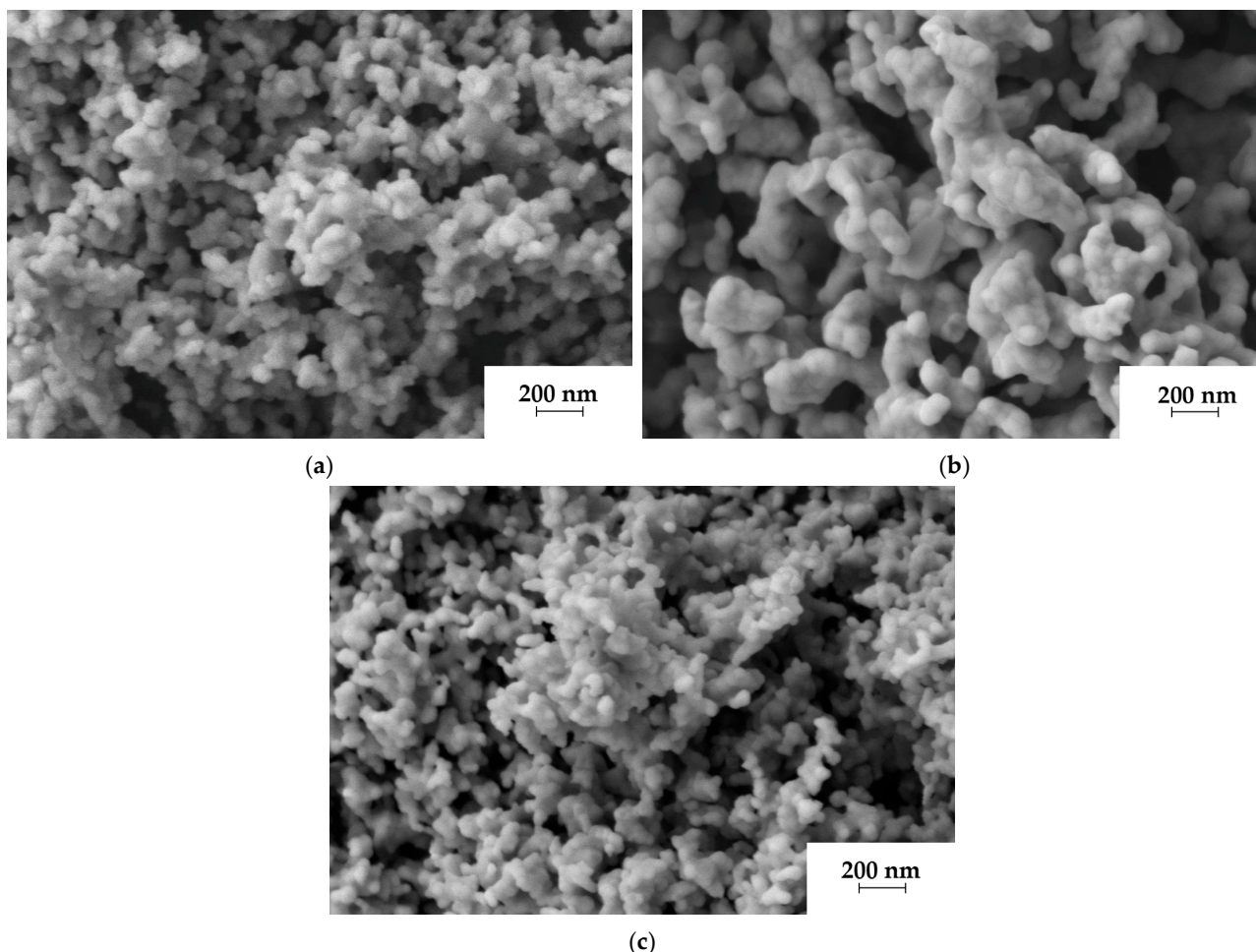


Figure 2. SEM images of SFAP powders obtained with (a) acetate, (b) chloride and (c) nitrate precursors.

To quantify the agglomeration degree of the powders, the so-called agglomeration coefficient (n) of particles was calculated from the formula [26] using the BET and XRD data:

$$n = (D_{\text{BET}}/D_{\text{XRD}}) \quad (1)$$

where D_{BET} is the average equivalent particle diameter corresponding to the measured specific surface area S_{BET} , and D_{XRD} is the calculated crystallite size based on the broadening of reflections in the X-ray diffraction patterns.

As can be seen from Table 1, the synthesized powders have almost identical crystallite sizes, while the dispersity increases from the chloride precursor to the nitrate one, which corresponds to the data of scanning electron microscopy. The specific surface area of the nitrate-derived powder is in good agreement with the data given in [12]. The difference of the agglomeration coefficient is mainly determined by the D_{BET} values. Since the minimum n value is observed for the nitrate-derived powders, they were selected for further study.

Table 1. Characteristics of SFAP powders derived from different precursors. S_{BET} —specific surface area, D_{BET} —average equivalent particle diameter, D_{XRD} —crystallite size, n —agglomeration coefficient.

Precursor	S_{BET}	D_{BET}	D_{XRD}	n
Strontium nitrate	15.1	96	30	3.2
Strontium acetate	10.9	132	35	3.8
Strontium chloride	8.5	170	33	5.1

2.2. Effect of Calcination Temperature on the Phase Composition of the SFAP Powders

Figure 3 shows the diffraction patterns of the obtained powders calcined at different temperatures. It was found that the characteristic diffraction peaks in the 2θ range of 20–60 degrees correspond to the hexagonal $\text{Sr}_5(\text{PO}_4)_3\text{F}$ structure (PDF# 50-1744) belonging to the P63/m space group (176). With an increase in the annealing temperature, the recrystallization of powders is observed, accompanied by an increase in the XRD peak intensities and a decrease in their widths. Secondary phase impurities were not detected at either intermediate or maximum temperatures.

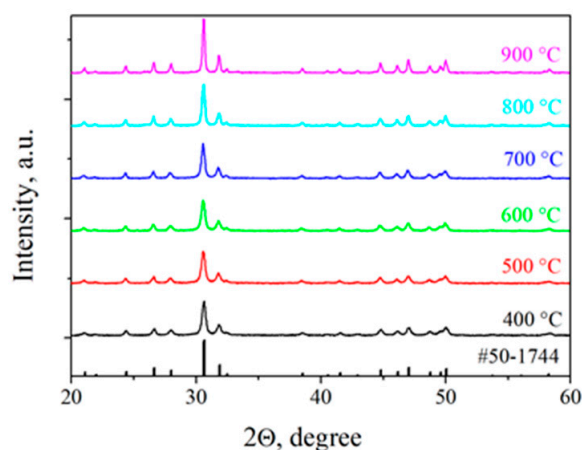


Figure 3. X-ray diffraction patterns of strontium nitrate-derived SFAP powders calcined at different temperatures. Vertical dashes—theoretical reflections for SFAP (PDF# 50-1744).

Based on the diffraction patterns, the unit cell parameters of the obtained crystalline phase were calculated. As can be seen from Table 2, the a and c values coincide within the confidence interval of the measurements and do not depend on calcination temperature. Using these values, the theoretical density of the material was found to be $\sim 4.14 \text{ g/cm}^3$, which is in good agreement with the previously published data [27].

Table 2. Parameters of the crystal structure of SFAP powders calcined at different temperatures.

Temperature, °C	a , Å	c , Å	V , Å ³	ρ , g/cm ³
400	9.71(2)	7.27(2)	593(4)	4.15(3)
500	9.71(3)	7.28(2)	595(4)	4.14(3)
600	9.71(2)	7.28(2)	595(4)	4.14(3)
700	9.72(2)	7.28(2)	596(3)	4.13(3)
800	9.71(2)	7.283(14)	595(2)	4.14(3)
900	9.715(10)	7.283(7)	595.3(13)	4.14(3)

2.3. Microstructure and Optical Properties of SFAP Ceramics

The SFAP powders calcined at 700 °C were chosen for ceramics sintering. Hot pressing was carried out in the temperature range of 900–1300 °C, which is the most often used to obtain fluorapatite ceramics [16–18].

The sample obtained at 900 °C was completely opaque, and the transmission spectra of the rest of the obtained ceramic samples in the visible and IR spectral regions are shown in Figure 4.

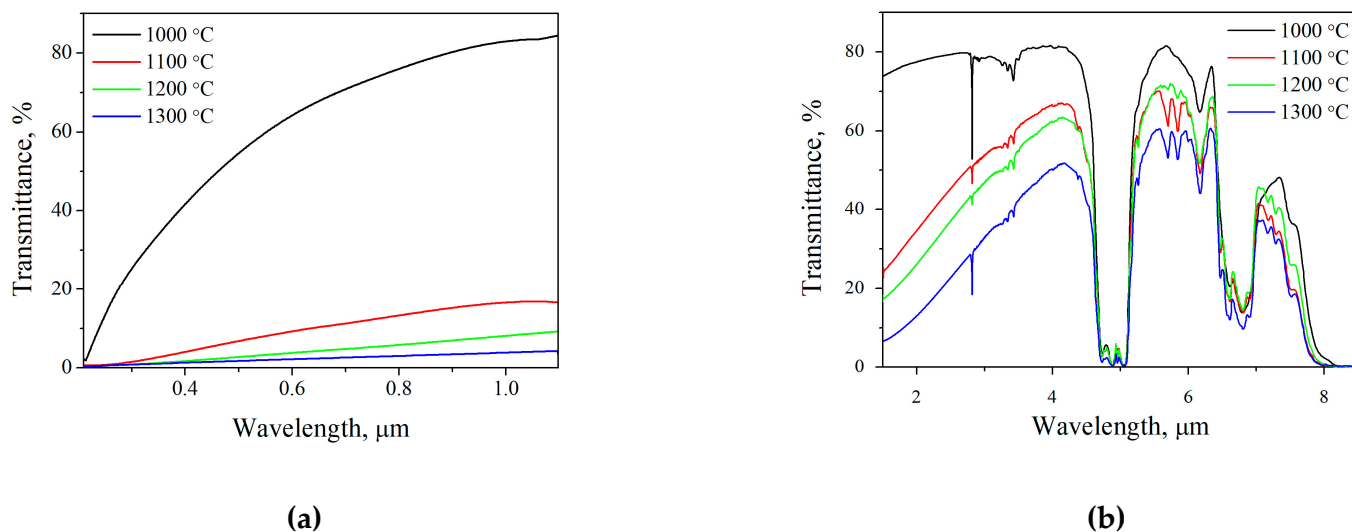


Figure 4. Transmission spectra of SFAP ceramics obtained by hot pressing at different temperatures in the (a) visible and (b) IR regions.

The short and long edges of the transmission window correspond to the wavelengths of 0.2 and ~ 8 μm . In the mid-IR range the transmission is 82%, which is one of the best results to date. A number of absorption bands are observed in the IR region. A sharp peak at 2.8 μm can be attributed to residual hydroxyl groups, which are able to isotropically replace the fluorine ion in the fluorapatite matrix; it corresponds to the spectrum published in [14,28,29]. According to [28,29], bands with a maximum at 2.80, 3.24, 3.34, 3.42, 5.71 and 5.84 μm could also be associated with the stretching vibrations of hydroxyl groups, while the absorption bands at 6.17 and 6.26 μm are associated with the bending vibrations of the hydroxyl groups. Intense bands in the region of 5 μm could be explained by the bending vibrations of PO_4 groups [28,29]. The incorporation of carbonate groups causes a broad absorption band at a 6.5–7 μm spectral range, which is due to the replacement of phosphate (type-B substitution) and in the apatite channels (A-type substitution) in the apatite structure [30]. The removal of these kinds of impurities is possible with the use of equipment capable of maintaining a higher level of vacuum. Closer to 8 μm , transparency is limited by a wide band of the matrix compounds, such as the asymmetric stretching vibrations (9.81 μm) and bending vibrations (10.58, 11.41 μm) of the P–O phosphate group [30].

The sample sintered at 1000 °C has the highest transmission over the entire range; apparently, this is due to the lowest scattering losses. This assumption is confirmed by the results of studying the microstructure of the obtained samples.

Figure 5 shows micrographs of the fractured surface of the ceramics sintered at different temperatures. It can be seen that the lowest sintering temperature does not ensure pores eliminating, while other samples have a dense microstructure. This agrees with the measured relative density of ceramics. When sintered at 900 °C, the SFAP density was $\sim 97\%$, while for the samples sintered at 1000–1300 degrees it exceeded 99.5%. The ceramics obtained at 1000 °C show the average grain size of ~ 150 nm, which provides the best optical properties.

An increase in the sintering temperature leads to a significant growth in grains. Thus, obtaining highly transparent SFAP ceramic samples should be carried out at temperatures no higher than 1000 °C. Otherwise, even an ideally dense structure of enlarged grains will cause radiation scattering.

Nevertheless, judging by the presence of scattering even in the best ceramic sample, further selection of the sintering period or the use of more complex two-stage modes is necessary to improve the microstructure of ceramics.

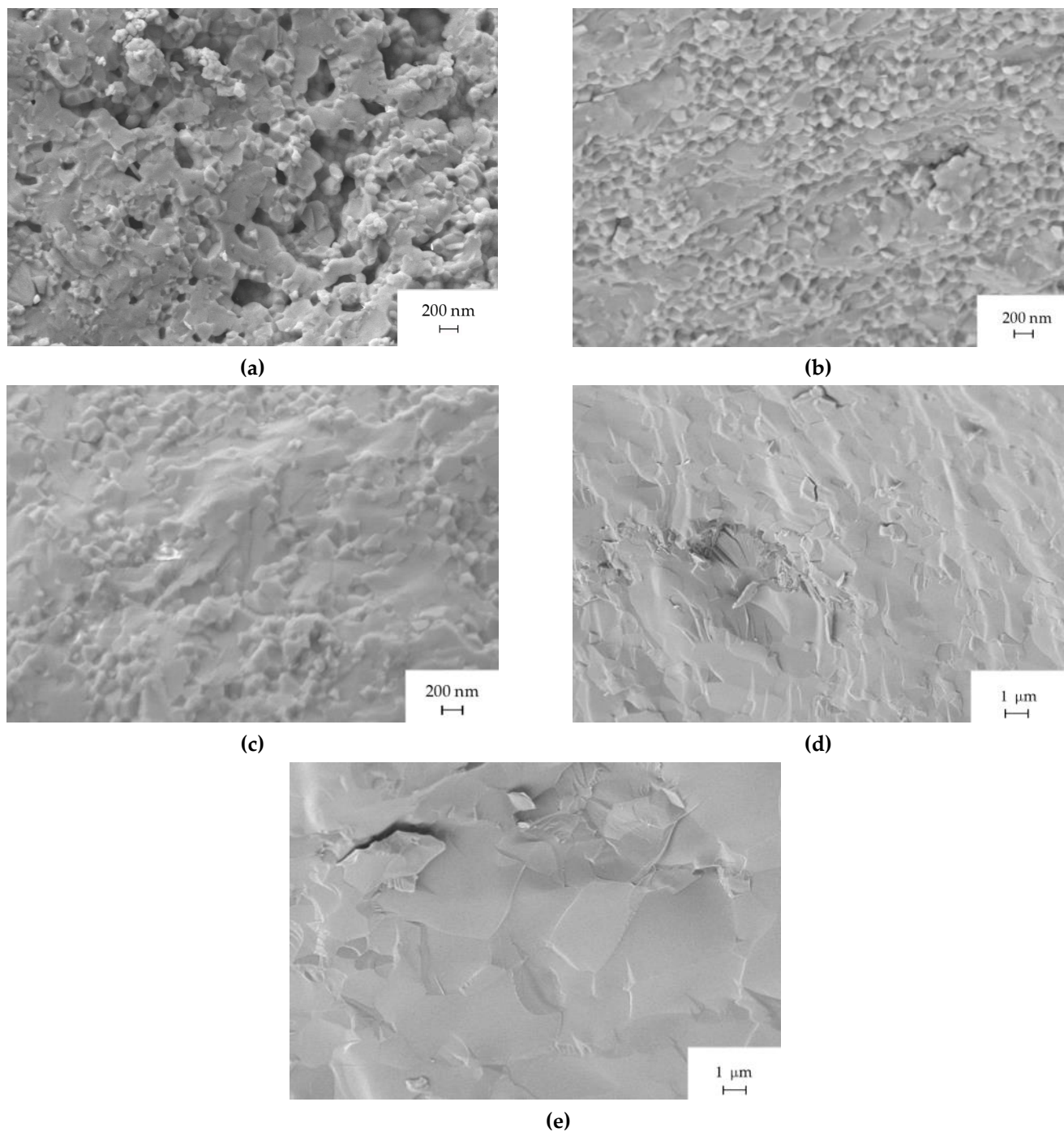


Figure 5. SEM images of SFAP ceramics obtained by hot pressing at (a) 900 °C, (b) 1000 °C, (c) 1100 °C (d) 1200 °C and (e) 1300 °C.

2.4. Luminescence of Erbium Ions in the SFAP Matrix

The main efforts in the study of FAP and SFAP ceramics are currently focused on obtaining materials doped with ytterbium and neodymium ions for the manufacture of lasers in the 1 μm range. Doping with erbium ions was carried out only when obtaining SFAP powders for the upconversion visualizers of IR radiation [31]. No data are given for the production of optical ceramics.

It was found that sintering under conditions similar to undoped SFAP does not lead to transparent samples; moreover, the Er:SFAP luminescence appears only in the region of 1.6 μm, and its intensity is extremely low. It turned out that it is possible

to increase the luminescence intensity by sintering Er:SFAP powders calcined at higher temperatures. However, the transmission of the ceramic increases insignificantly in this case. The luminescence spectra of 2% Er:SFAP ceramics, produced from powders calcined at different temperatures, in the wavelength range of 1.45–1.65 μm corresponding to the $^4I_{13/2} \rightarrow ^4I_{15/2}$ transition, are shown in Figure 6. As can be seen, the IR luminescence intensity rises when increasing the temperature at which the samples are calcined.

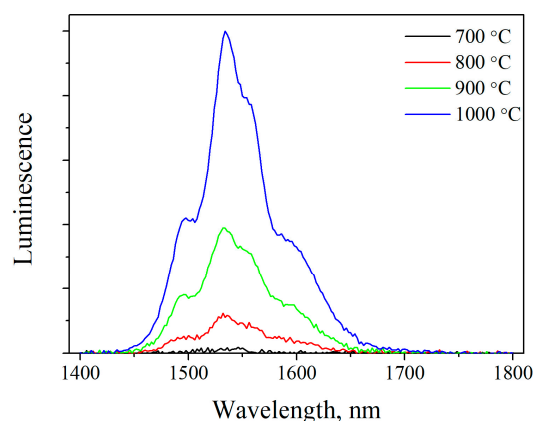


Figure 6. Luminescence of 2% Er:SFAP ceramics sintered with powders annealed at different temperatures.

This fact correlates with the results obtained in [31,32], where it was found that ErYb:SFAP powders do not exhibit luminescence if their calcination temperature does not exceed 850–900 $^{\circ}\text{C}$. The authors attribute this to the point lattice defects that arise due to the lack of compensation for the valence of triply-charged rare-earth ions in the SFAP matrix. Calcination at higher temperatures leads to the substitution of a part of the fluoride ions by oxygen, which equalizes the ion balance and promotes luminescence.

The presence of residual OH-groups will also affect the luminescence. In addition to the resonant absorption of the luminescence of erbium ions in the region of 3 μm , hydroxyl groups can act as acceptors and significantly reduce the intensity and lifetime of luminescence, as it was shown, for example, for Yb:Sc₂O₃ [33]. Moreover, OH-groups can contribute to the elimination of fluorine via $\text{OH}^- + \text{F}^- \rightarrow \text{O}^{2-} + \text{HF}$ reaction.

Figure 7a shows the luminescence decay kinetics of Er:SFAP ceramics hot pressed with powders calcined at different temperatures. At a low temperature (700 $^{\circ}\text{C}$), the process can be divided into two stages with rapid decay in the beginning. With an increase in temperature, the dependence becomes more linear. This fact can be attributed to a lower impurities content (such as hydroxyl groups) and higher crystallinity. The curve of the sample calcined at 1000 $^{\circ}\text{C}$ is approximated by a single exponent, as shown in Figure 7b. The lifetime of Er³⁺ ions calculated from these data amounted to 5 ms. The resulting value is ~ 2 times lower than that measured for single-crystal Er:SFAP [34]. Apparently, this difference is due to a significantly higher content of erbium –2% vs. 0.15% for monocrystal. Compared with previously studied materials, we can say that the obtained value is on the same level with such known media as scandium oxide and lithium niobate [35].

When discussing the reasons for the opacity of Er:SFAP ceramics, we made an assumption about the formation of a secondary phase of the rare earth element. For this purpose, the X-ray diffraction patterns of ceramics obtained from the powders calcined from 700 to 1000 $^{\circ}\text{C}$ were recorded. As can be seen from Figure 8, calcination at 700 $^{\circ}\text{C}$ does not lead to the formation of a secondary phase, while at 1000 $^{\circ}\text{C}$ a small peak with a maximum of 33.36 degrees appears, which can be identified as one of the most intense peaks for Sr₃Er(PO₄)₃ (PDF card # 33-1328). Thus, Er:SFAP is a promising material for the manufacture of eye-safe laser materials; however, it is necessary to carefully optimize the temperature and the powder processing environment to prevent decomposition of the SFAP phase.

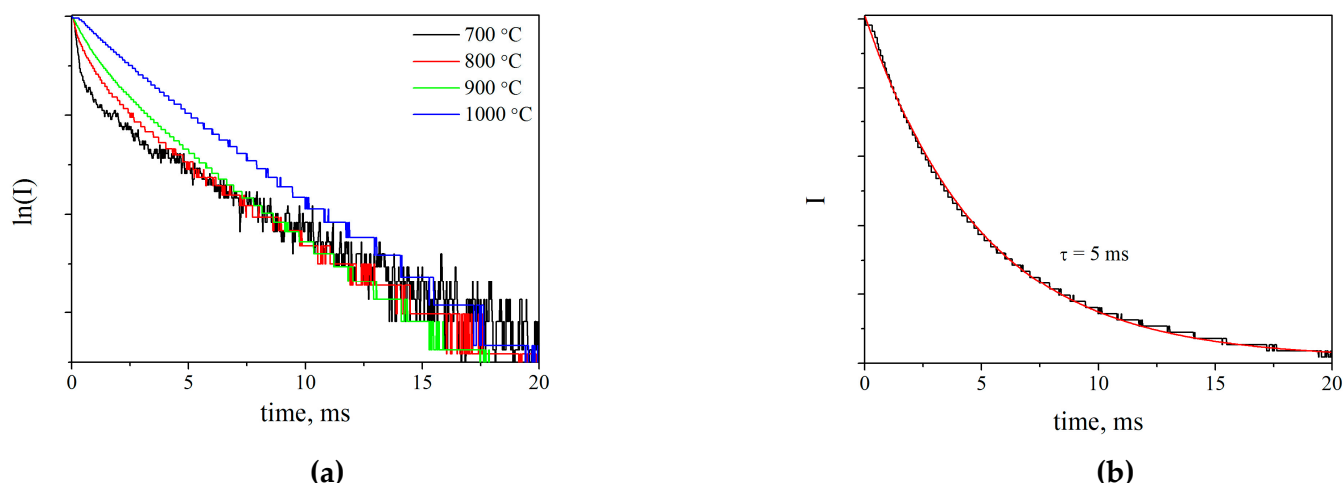


Figure 7. (a) Luminescence decay curves of erbium ions in SFAP ceramics from the powders calcined at different temperatures and (b) exponential fitting of the luminescence decay for Er:SFAP calcined at 1000 °C.

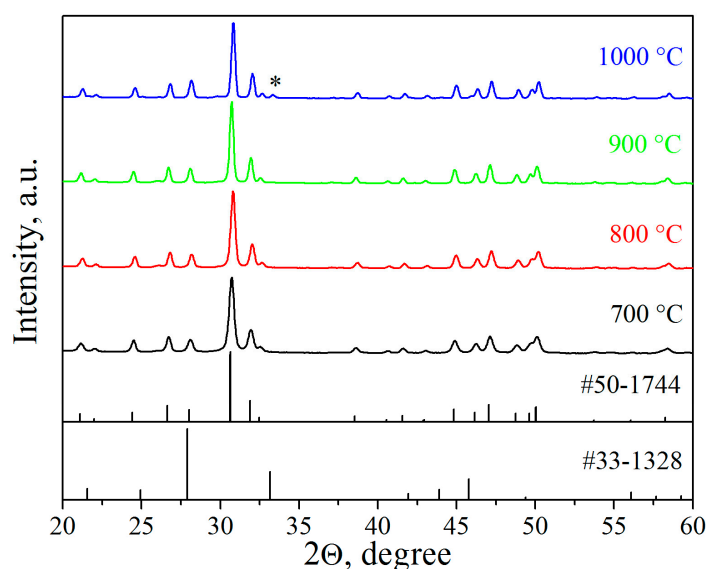


Figure 8. X-ray diffraction patterns of Er:SFAP powders calcined at different temperatures. Vertical dashes—theoretical reflections for SFAP (PDF# 50-1744) and $\text{Sr}_3\text{Er}(\text{PO}_4)_3$ (PDF # 33-1328).

3. Materials and Methods

To obtain strontium fluorapatite (SFAP) nanopowders doped with erbium ions, strontium carbonate SrCO_3 (II) (99.9%, Khimreaktiv, N. Novgorod, Russia); ammonium hydrogen phosphate $(\text{NH}_4)_2\text{HPO}_4$ (99.5%, Khimreaktiv); ammonium fluoride NH_4F (99.9%, Vekton); nitric acid HNO_3 (99.999%, Khimreaktiv); hydrochloric acid HCl (99.999%, Khimreaktiv); acetic acid CH_3COOH (99.9%, Khimreaktiv); ammonium hydroxide NH_4OH (99.999%, Khimreaktiv); and erbium oxide Er_2O_3 (99.999%, Polirite, Moscow, Russia) were used as starting materials.

Figure 9 shows a flowchart for the synthesis of SFAP powders. First, strontium carbonate was dissolved in nitric, hydrochloric or acetic acid to obtain 0.3 M solutions of strontium nitrate, chloride and acetate, respectively. To eliminate residual carbonate ions, the solution was degassed by boiling for 2 h on a magnetic stirrer.

Nanopowders of $\text{Sr}_5(\text{PO}_4)_3\text{F}$ were obtained by direct-strike precipitation. To a cationic solution containing 0.035 mol of strontium ions, a solution of a precipitant containing

0.021 mol of ammonium hydrogen phosphate, 0.007 mol of ammonium fluoride and 0.021 mol of ammonium hydroxide was added dropwise with a 2 mL/min rate under constant stirring.

The corresponding scheme of the proceeding chemical reactions could be written as follows:

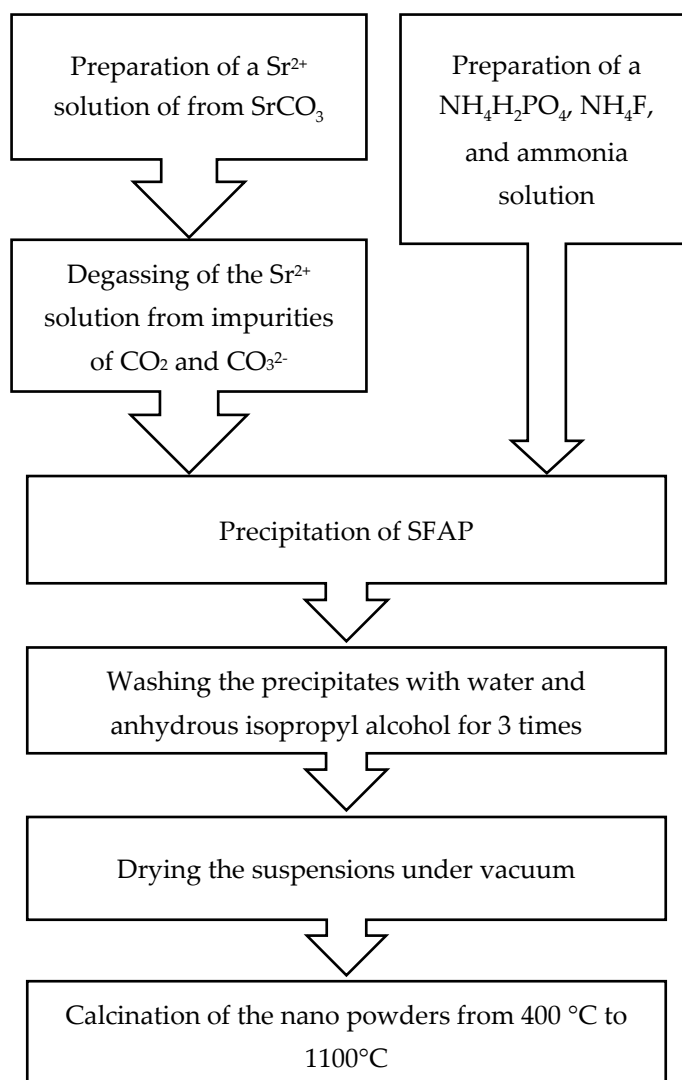
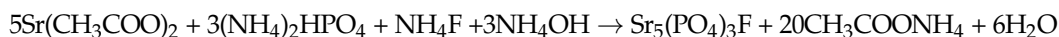
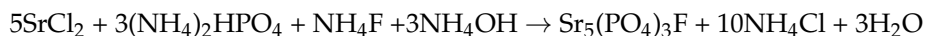


Figure 9. Flowchart for the synthesis of SFAP powders.

To obtain the powder of a required phase and at a minimum agglomeration degree, in accordance with the literature data [12], the pH of the medium was maintained with ammonium hydroxide in the range of 7–8. This is crucial since at lower pH values, the formation of strontium fluoride could occur, and in an alkaline solution, hydroxyl groups replace fluorine ions more intensively. The resulting suspension was kept under constant stirring for 24 h. Then, the precipitates were washed three times with deionized water and three times with anhydrous isopropyl alcohol and dried in a vacuum oven at 60 °C for 5 h at a residual pressure of 0.5 bar. After that, the precipitates were calcined in a muffle furnace at temperatures from 400 to 1100 °C in a muffle furnace.

To obtain Er-doped SFAP powders, the initial erbium oxide was dissolved in a stoichiometric amount of nitric acid, and the resulting solution was added to the solution of strontium ions. The mole fraction of the dopant was 2 mol %.

The morphology and structural properties of the synthesized nanopowders were studied using the methods of electron microscopy, X-ray diffraction analysis (XRD) and BET adsorption-structural analysis. This made it possible to correctly assess the main characteristics of the powders—dispersity and phase composition, and the degree of agglomeration.

The XRD analysis of the nanopowders was carried out on an XRD-6000 diffractometer (Shimadzu, Japan) equipped with a graphite monochromator (CuK α radiation $\lambda = 1.54178 \text{ \AA}$) in the 2θ range of 15° – 65° . The scanning step for 2θ was 0.02° , the scanning rate was $2^\circ/\text{min}$. The ICDD database was used in the analysis.

The average crystallite size of D_{XRD} was evaluated using the Scherrer equation: $D_{XRD} = 0.9\lambda/(\beta\cos\theta)$, where λ is the CuK α wavelength and β is the full width at half maximum of the diffraction peak at the Bragg angle θ .

The cell parameters were calculated by the Rietveld method using the «Diffrac.TOPAS» software (Bruker, Germany) with the cif-file from the ICSD database (2016), deposition No. 95737. Theoretical density was calculated from the results of the XRD analysis using the formula:

$$\rho_{XRD} = \frac{Z \cdot M \cdot 1.66}{V} \quad (2)$$

where Z is the number of structural units in the unit cell, M —average molar mass, V —the unit cell volume.

The morphology of the powders and the microstructure of the sintered ceramics were studied on an Auriga CrossBeam scanning electron microscope (Carl Zeiss, Germany) at an accelerating beam voltage of 3 keV with a secondary electron detector.

The specific surface area (S_{BET}) of the SFAP nanopowders was measured using the Brunauer–Emmett–Teller (BET) method on a Sorbi-MS (Meta, Russia) instrument. The measurements were carried out on powders calcined at 800°C . The average particle diameter (D_{BET}) was calculated based on the assumption of its spherical shape, according to the equation:

$$D_{BET} = \frac{6}{\rho \times S_{BET}} \quad (3)$$

where ρ is the theoretical density of the material, calculated from the X-ray diffraction patterns.

The powders were consolidated by hot pressing in a vacuum in a graphite mold ($\varnothing 15 \text{ mm}$), at maximum temperatures of 1000 – 1300°C and a uniaxial pressure of 50 MPa , on homemade equipment. The soaking time at maximum temperature was set for 10 min . Prior to sintering, the powder was compacted in a stainless steel mold at a pressure of $\sim 10 \text{ MPa}$. The compacted material was isolated with graphite paper in order to reduce the contamination effect of the equipment and to minimize the adhesion of the ceramic sample to the surface of the punch. Heating was carried out with the use of graphite heaters; the residual pressure in the chamber was not more than 10 Pa .

The obtained ceramic samples were ground and polished on both sides to a thickness of 0.5 mm using diamond slurry. The relative density of the ceramic samples was determined by hydrostatic weighing in water. The optical transmission spectra of the ceramics in the visible and IR ranges were measured using an SF-2000 spectrophotometer (LOMO, Russia) (190 – 1100 nm) and FT-801 IR Fourier spectrometer (SIMEX, Russia).

The luminescence of the SFAP ceramic samples doped with erbium ions was excited by a laser diode at a wavelength of 975 nm , and the spectra were recorded using the SOLAR TII S150-2 spectrometer. The luminescence spectra of the Er:SFAP powders were measured using an automated setup based on the SOLAR M833 monochromator and the SRS SR830 lock-in amplifier, under excitation of the 975 nm diode laser. Infrared luminescence was recorded using the Thorlabs PDA30G photodetector equipped with silicon and germanium filters.

The luminescence decay of Er^{3+} ions in the range of 1.55 μm was studied upon excitation by laser pulses with a fall time of about 10 μs . The dependence was approximated by the exponent decay function: $y = A_1 \cdot \exp(-x/t_1)$.

4. Conclusions

1. The effect of a strontium source on the morphological properties of SFAP powders was studied; it was established that the powders obtained using strontium nitrate have the lowest agglomeration coefficient.

2. The influence of the calcination temperature on the parameters of the crystal structure of SFAP powders was determined. Sufficient recrystallization was observed while the unit cell parameters do not depend on temperature.

3. It was shown that hot pressing of the obtained powders at a temperature of 1000 $^{\circ}\text{C}$ and an external pressure of 50 MPa makes it possible to form a non-porous microstructure with a characteristic grain size of ~ 150 nm. This ensures the transmission of ceramics in the visible and IR ranges; however, the transmission spectra contain a large number of impurity absorption bands.

4. The introduction of an active additive of erbium oxide in the amount of 2 mol % leads to the formation of a secondary phase at annealing temperatures above 900 $^{\circ}\text{C}$, which limits the transmission of Er:SFAP ceramics. At the same time, when the resulting ceramics are pumped with a diode laser at 975 nm, intense luminescence is observed in the region of 1.5–1.7 μm .

Author Contributions: Investigation, D.P., M.N., S.K., S.B., A.B., V.K. and A.N.; writing—original draft preparation, M.N., D.P., V.K. and A.N.; writing—review and editing, S.B., D.P. and A.B. All authors have read and agreed to the published version of the manuscript.

Funding: This research was funded with the “Priority 2030” program at the N.I. Lobachevsky National Research University, grant No N-463-99_2021-2023.

Institutional Review Board Statement: Not applicable.

Informed Consent Statement: Not applicable.

Data Availability Statement: Not applicable.

Conflicts of Interest: The authors declare no conflict of interest.

References

1. Erlandson, A.; Aceves, S.; Bayramian, A.; Bullington, A.; Beach, R.; Boley, C.; Caird, J.; Deri, R.; Dunne, A.; Flowers, D.; et al. Comparison of Nd:phosphate glass, Yb:YAG and Yb:S-FAP laser beamlines for laser inertial fusion energy (LIFE). *Opt. Mater. Express*. **2011**, *1*, 1341–1352. [[CrossRef](#)]
2. Steinbruegge, K.; Henningsen, T.; Hopkins, R.; Mazelsky, R.; Melamed, N.; Riedel, E.; Roland, G. Laser Properties of Nd³⁺ and Ho³⁺ Doped Crystals with the Apatite Structure. *Appl. Opt.* **1972**, *11*, 999–1012. [[CrossRef](#)] [[PubMed](#)]
3. Schaffers, K.; Tassano, J.; Bayramian, A.; Morris, R. Growth of Yb: S-FAP [Yb³⁺:Sr₅(PO₄)₃F] crystals for the Mercury laser. *J. Cryst. Growth*. **2003**, *253*, 297–306. [[CrossRef](#)]
4. Schaffers, K. Yb:S-FAP lasers. *Opt. Mater.* **2004**, *26*, 391–394. [[CrossRef](#)]
5. Schaffers, K.; Bayramian, A.; Marshall, C.; Tassano, J.; Payne, S. Analysis of Sr_{5-x}Ba_x(PO₄)₃F:Yb³⁺ crystals for improved laser performance with diode-pumping. In *Advanced Solid State Lasers*; Pollock, B., Bosenberg, W., Eds.; Optica Publishing Group: Orlando, FL, USA, 1997; p. SC4. [[CrossRef](#)]
6. Marshall, C.; Payne, S.; Smith, L.; Beach, R.; Emanuel, M.; Skidmore, J.; Powell, H.; Krupke, W.; Chai, B. Diode-Pumped Yb:Sr₅(PO₄)₃F Laser Performance. In *Advanced Solid State Lasers*; Chai, B., Payne, S., Eds.; Optica Publishing Group: Memphis, TN, USA, 1995; p. YL2. [[CrossRef](#)]
7. Yagi, H.; Takaichi, K.; Ueda, K.; Yamasaki, Y.; Yanagitani, T.; Kaminskii, A. The physical properties of composite YAG ceramics. *Laser Phys.* **2005**, *15*, 1338–1344.
8. Gavrishchuk, E.; Ikonnikov, V.; Kazantsev, S.; Kononov, I.; Rodin, S.; Savin, D.; Timofeeva, N.; Firsov, K. Scaling of energy characteristics of polycrystalline laser at room temperature. *Quantum Electron.* **2015**, *45*, 823. [[CrossRef](#)]
9. Kuznetsov, S.; Alexandrov, A.; Fedorov, P. Optical Fluoride Nanoceramics. *Inorg. Mater.* **2021**, *57*, 555–578. [[CrossRef](#)]
10. Akiyama, J.; Sato, Y.; Taira, T. Laser ceramics with rare-earth-doped anisotropic materials. *Opt. Lett.* **2010**, *35*, 3598–3600. [[CrossRef](#)]

11. Sato, Y.; Arzakantsyan, M.; Akiyama, J.; Taira, T. Anisotropic Yb:FAP laser ceramics by micro-domain control. *Opt. Mater. Express.* **2014**, *4*, 2006–2015. [[CrossRef](#)]
12. Chai, B.; Hao, L.; Mao, X.; Xu, X.; Li, X.; Jiang, B.; Zhang, L. Precipitation and Growth Mechanism of Diverse Sr₅(PO₄)₃F Particles. *J. Am. Ceram. Soc.* **2016**, *99*, 1498–1503. [[CrossRef](#)]
13. Wu, Y.; Du, J.; Clark, R. Synthesis of Yb³⁺ doped Sr₅(PO₄)₃F nanoparticles through co-precipitation. *Mater. Lett.* **2013**, *107*, 68–70. [[CrossRef](#)]
14. Wu, Y. Nanostructured transparent ceramics with an anisotropic crystalline structure. *Opt. Mater. Express.* **2014**, *4*, 2026–2031. [[CrossRef](#)]
15. Liu, X.; Tan, G.; Zhou, Z.; Mei, B. Fabrication, microstructure, mechanical and luminescence properties of transparent Yb³⁺-doped Sr₅(PO₄)₃F nanostructured ceramics. *J. Eur. Ceram. Soc.* **2022**, *42*, 6642–6653. [[CrossRef](#)]
16. Liu, X.; Tan, G.; Li, W.; Mei, B. Conventional HP sintering of asymmetric hexagonal structure Yb³⁺-doped Sr₅(PO₄)₃F transparent ceramic without additives. *J. Am. Ceram. Soc.* **2022**, *105*, 4581–4587. [[CrossRef](#)]
17. Zhang, Y.; Mei, B.; Li, W.; Yang, Y.; Yi, G.; Zhou, Z.; Liu, Z. Fabrication and spectral properties of Nd:S-FAP transparent ceramics by simple route of HP method. *J. Alloys Compd.* **2020**, *820*, 153171. [[CrossRef](#)]
18. Zhang, Y.; Zhou, Z.; Mei, B.; Yang, Y. The effect of Y³⁺ doping upon Nd: S-FAP transparent ceramics for effective spectral performance improvement. *Ceram. Int.* **2022**, *49*, 1362–1368. [[CrossRef](#)]
19. Furuse, H.; Horiuchi, N.; Kim, B.-N. Transparent non-cubic laser ceramics with fine microstructure. *Sci. Rep.* **2019**, *9*, 10300. [[CrossRef](#)]
20. Furuse, H.; Okabe, T.; Shirato, H.; Kato, D.; Horiuchi, N.; Morita, K.; Kim, B.-N. High-optical-quality non-cubic Yb³⁺-doped Ca₁₀(PO₄)₆F₂ (Yb:FAP) laser ceramics. *Opt. Mater. Express.* **2021**, *11*, 1756–1762. [[CrossRef](#)]
21. Zhmykhov, V.; Dobretsova, E.; Tsvetkov, V.; Nikova, M.; Chikulina, I.; Vakalov, D.; Tarala, V.; Pyrkov, Y.; Kuznetsov, S.; Tsvetkov, V. Judd-Ofelt Analysis of High Erbium Content Yttrium-Aluminum and Yttrium-Scandium-Aluminum Garnet Ceramics. *Inorganics* **2022**, *10*, 170. [[CrossRef](#)]
22. Chaika, M.; Balabanov, S.; Permin, D. Optical spectra and gain properties of Er³⁺:Lu₂O₃ ceramics for eye-safe 1.5-μm lasers. *Opt. Mater.* **2021**, *112*, 110785. [[CrossRef](#)]
23. Liu, J.; Liu, P.; Wang, J.; Xu, X.; Li, D.; Zhang, J.; Nie, X. Fabrication and Sintering Behavior of Er:SrF₂ Transparent Ceramics using Chemically Derived Powder. *Materials* **2018**, *11*, 475. [[CrossRef](#)] [[PubMed](#)]
24. Šulc, J.; Němec, M.; Švejkar, R.; Jelínková, H.; Doroshenko, M.; Fedorov, P.; Osiko, V. Diode-pumped Er:CaF₂ ceramic 2.7 μm tunable laser. *Opt. Lett.* **2013**, *38*, 3406–3409. [[CrossRef](#)] [[PubMed](#)]
25. Basiev, T.T.; Orlovskii, Y.V.; Polyachenkova, M.V.; Fedorov, P.P.; Kuznetsov, S.V.; Konyushkin, V.A.; Osiko, V.V.; Alimov, O.K.; Dergachev, A.Y. Continuously tunable cw lasing near 2.75 μm in diode-pumped Er³⁺: SrF₂ and Er³⁺: CaF₂ crystals. *Quantum Electron* **2006**, *36*, 591–594. [[CrossRef](#)]
26. Malyavin, F.; Tarala, V.; Kuznetsov, S.; Kravtsov, A.; Chikulina, I.; Shama, M.; Medyanik, E.; Ziryanov, V.; Evtushenko, E.; Vakalov, D.; et al. Influence of the ceramic powder morphology and forming conditions on the optical transmittance of YAG:Yb ceramics. *Ceram. Int.* **2019**, *45*, 4418–4423. [[CrossRef](#)]
27. Grisafe, D.A.; Hummel, F.A. Pentavalent Ion Substitutions in the Apatite Structure Part A. Crystal Chemistry. *J. Solid State Chem.* **1970**, *2*, 160–166. [[CrossRef](#)]
28. Marincea, Ș.; Dumitraș, D.-G.; Sava Ghineț, C.; Dal Bo, F. Carbonate-Bearing, F-Overcompensated Fluorapatite in Magnesian Exoskarns from Valea Rea, Budureasa, Romania. *Minerals* **2022**, *12*, 1083. [[CrossRef](#)]
29. Baddiel, C.; Berry, E. Spectra structure correlations in hydroxy and fluorapatite. *Spectrochim. Acta.* **1966**, *22*, 1407–1416. [[CrossRef](#)]
30. Weidner, V.; Carney, M.; Schermerhorn, D.; Pasteris, J.; Yoder, C. A-type substitution in carbonated strontium fluor-, chlor- and hydroxylapatites. *Mineral. Mag.* **2015**, *79*, 399–412. [[CrossRef](#)]
31. Grigorjeva, L.; Smits, K.; Millers, D.; Jankoviča, D. Luminescence of Er/Yb and Tm/Yb doped FAp nanoparticles and ceramics, IOP Conf. Ser. Mater. Sci. Eng. **2015**, *77*, 12036. [[CrossRef](#)]
32. Li, X.; Zhu, J.; Man, Z.; Ao, Y.; Chen, H. Investigation on the structure and upconversion fluorescence of Yb³⁺/Ho³⁺ co-doped fluorapatite crystals for potential biomedical applications. *Sci. Rep.* **2014**, *4*, 4446. [[CrossRef](#)]
33. Permin, D.; Kurashkin, S.; Novikova, A.; Savikin, A.; Gavrishchuk, E.; Balabanov, S.; Khamaletdinova, N. Synthesis and luminescence properties of Yb-doped Y₂O₃, Sc₂O₃ and Lu₂O₃ solid solutions nanopowders. *Opt. Mater.* **2018**, *77*, 240–245. [[CrossRef](#)]
34. Gruber, J.B.; Wright, A.O.; Seltzer, M.D.; Zandi, B.; Merkle, L.D.; Hutchinson, J.A.; Morrison, C.A.; Allik, T.H.; Chai, B.H.T. Site-Selective Excitation and Polarized Absorption and Emission Spectra of Trivalent Thulium and Erbium in Strontium Fluorapatite. *J. Appl. Phys.* **1997**, *81*, 6585–6598. [[CrossRef](#)]
35. Gheorghie, C.; Georgescu, S.; Lupei, V.; Lupei, A.; Ikesue, A. Absorption intensities and emission cross section of Er³⁺ in Sc₂O₃ transparent ceramics. *J. Appl. Phys.* **2008**, *103*, 83116. [[CrossRef](#)]

Disclaimer/Publisher's Note: The statements, opinions and data contained in all publications are solely those of the individual author(s) and contributor(s) and not of MDPI and/or the editor(s). MDPI and/or the editor(s) disclaim responsibility for any injury to people or property resulting from any ideas, methods, instructions or products referred to in the content.